Hindawi Publishing Corporation
Mathematical Problems in Engineering
Volume 2010, Article ID 191898, 22 pages
doi:10.1155/2010/191898

Research Article

Investigations on Actuator Dynamics through Theoretical and Finite Element Approach

Somashekhar S. Hiremath and M. Singaperumal

Precision Engineering and Instrumentation Laboratory, Department of Mechanical Engineering, Indian Institute of Technology Madras, Chennai 6000 36, India

Correspondence should be addressed to M. Singaperumal, msingam@iitm.ac.in

Received 29 July 2009; Accepted 23 October 2009

Academic Editor: Yuri Vladimirovich Mikhlin

This paper gives a new approach for modeling the fluid-structure interaction of servovalve component-actuator. The analyzed valve is a precision flow control valve-jet pipe electrohydraulic servovalve. The positioning of an actuator depends upon the flow rate from control ports, in turn depends on the spool position. Theoretical investigation is made for No-load condition and Load condition for an actuator. These are used in finite element modeling of an actuator. The fluid-structure-interaction (FSI) is established between the piston and the fluid cavities at the piston end. The fluid cavities were modeled with special purpose hydrostatic fluid elements while the piston is modeled with brick elements. The finite element method is used to simulate the variation of cavity pressure, cavity volume, mass flow rate, and the actuator velocity. The finite element analysis is extended to study the system's linearized response to harmonic excitation using direct solution steady-state dynamics. It was observed from the analysis that the natural frequency of the actuator depends upon the position of the piston in the cylinder. This is a close match with theoretical and simulation results. The effect of bulk modulus is also presented in the paper.

1. Introduction

The electrohydraulic servovalves (EHSVs), probably the youngest of the standard hydraulic components, made it appearance in the latter 1940s to satisfy the aerospace needs for a fast response servo-controlled system. After 1940s these EHSVs were not significantly faster than electrical servos because they were lacking by an element which could rapidly translate electrical signals into a hydraulic flows. These early servovalves were actuated by small electric servomotors with a large time constants and hence they are the slowest element in the control loop and have a limited system performance. In the early 1950s permanent magnet torque motors having fast response gained favor as a method of stroking valves and the EHSV took its present form. EHSV connects the electronic and hydromechanical portions of a system and hence it is treated as a mechatronic component.

EHSVs are faster responding directional, pressure, and flow control valves, which are frequently used in closed-loop control arrangements to produce the highly sophisticated performance, in terms of high-frequency response, required by modern machines. They serve as an interface between electrical devices and hydraulic systems. They are capable of converting low-power electrical input into movement of spool to precisely control large power, low-speed hydraulic actuators. Thus, they are extensively used in such applications as computer numerical controlled machine tools, aircraft, robotic manipulators, motion simulators, injection molding, remotely controlled mechanisms, and many off-highway and mobile applications.

Most present day EHSVs have three major components:

(1) torque motor,

(2) first-stage hydraulic amplifier,

(3) second-stage sliding spool valve.

The torque motor consists of an armature mounted on a torsion pin pivot and suspended in the air gap of a magnetic field. Two pole pieces, one permanently polarized north and the other south by the permanent magnet, form the framework around the armature and provide paths for the magnetic flux. When current is made to flow through the armature coils, the armature ends become polarized and each end is attracted to one pole piece and repelled by the other. A torque thus produced rotates the armature proportional to the input current. The servovalve to be positioned may be mechanically attached at either armature end. The static and dynamic characteristic of the torque motor plays a vital role in EHSV operation and is well elaborated in the books [1, 2]. Maskrey and Thayer [3] elaborated the historical development, market growth, and wide application areas of EHSV. The selection and performance criteria for electrohydraulic servodrives are given Moog technical bulletin 122 [4] and the performance estimation for electrohydraulic control systems are given Moog technical bulletin 126 [5].

First-stage hydraulic amplifier substantially multiplies the force output of the torque motor to a level sufficient to overcome considerable flow forces, stiction forces, and forces resulting from the acceleration or vibration. Flapper, jet pipe, and spool valves may be used as a hydraulic amplifier in EHSV. Much of the work has been done to study dynamics of flapper/nozzle EHSV. The design aspects and various configurations of EHSV particularly on flapper/nozzle are available in many text books [1, 2, 6–9].

Second-stage sliding spool valves are classified based on many parameters.

(i) *Number of ways "flow" can enter and leave the valve.* Generally all servovalves require at least one supply port, one return port and one line to the load and hence they are classified as a three-way EHSV or a four-way EHSV.

(ii) *Number of spool lands*. The number of lands on a spool may vary from one in a primitive valve to the usual three or four, and special valves may have as many as six lands.

(iii) *Type of valve center when the spool is in neutral position.* If the width of the spool land is smaller than the control port width in the valve sleeve, the valve is said to have an open center or to be an under lapped. If the width of the spool land is identical to the control port width in the valve sleeve, the valve is said to have a critical center or a zero lapped. If the width of the spool land is greater than the control port width in the valve sleeve, the valve is said to have a closed center or to be an overlapped.

The flow forces on the spool dynamics of flapper/nozzle EHSV and their compensation methods are elaborated by Lee and Blackburn [10]. Taft and Twill [11] developed a flow model of a three-way underlapped hydraulic servovalve and derived a mathematical description of the flow momentum forces acting on the spool valve. The effect of these forces on valve performance is investigated by examining both the linearized system of differential equations and digital computer solutions of the system nonlinear differential equations, and by experimental measurements. Lee et al. [12] developed a new linearized equation for modeling servovalve as a modified form of the conventional linearized equation. The conventional linearized equation described by the first-order terms of Taylor's series is effective just near the operating point. However, pressure and flow rate in actual hydraulic systems are usually not confined near an operating point. From the evaluations of time responses and frequency responses obtained from simulations for a hydraulic control system, the effectiveness of the new linearized equation and the methods to determine effective operating points is confirmed.

A detailed transfer function of the flapper/nozzle EHSV has been developed and simulated by Nikiforuk et al. [13]. LeQuoc et al. [14] proposed a novel electrohydraulic configuration, in which the drain line is connected to the tank through a direction control valve, a metering valve, and a relief valve which allow external adjustment of the drain, orifice and back pressure. Servosystems with the conventional servovalve and the new servovalve configuration are modeled and simulated for step input for various values of system parameters. The simulation results indicated that the servosystem with this new configuration would offer a higher steady-state velocity, a lower percent overshoot, and a lesser settling time, if the drain line orifice opening and the back pressure were properly tuned. Also they carried out experiments to validate the simulation results and it has been demonstrated that the mathematical model is relatively adequate to predict the performance of the two servosystems.

Das et al. [15] modeled the electrohydraulic actuation system used for launch vehicle attitude control. The unified nonlinear model has been developed taking into account the associated nonlinearities. The developed model has been simulated using the Matlab and the simulation results are compared with experimental values.

However, studies on jet pipe EHSV are limited. Jet pipe EHSV finds main applications in jet engine, flight control, and turbofan engine control system. Fredlake and Adams [16], Bruce [17], and Harschburger [18] worked on the development of flight control system for fighter aircrafts and hydromechanical control. Ogata [19] explained the operation of a hydraulic jet pipe controller and how the jet pipe controller governs the position of the butterfly valve.

The basic components and principle of operation of jet pipe EHSV are available in text books [1, 2, 6–9]. The major parameters affecting the first-stage pressure recovery are presented by Allen [1]. Experimentally these pressure recoveries in the receiver holes have been measured and studied the valve dynamics using the frequency response method as detailed by Dushkes and Cahn [20]. The pressure recoveries in the receiver holes have been simulated using a bond graph method—a dynamic model tool, and the spool dynamics is studied by Thoma [21]. An analytical and experimental investigation of a jet pipe—controlled electropneumatic servoactuator designed for use in the Utah/MIT dextrous hand has been performed by Henri et al. [22].

The modification in the jet pipe EHSV results in a new design called the deflector jet EHSV. The design aspects and operating principle of the deflector jet EHSV are elaborated in Moog technical bulletin 121 [23]. The jet pipe EHSV is not used as much as the flapper/nozzle

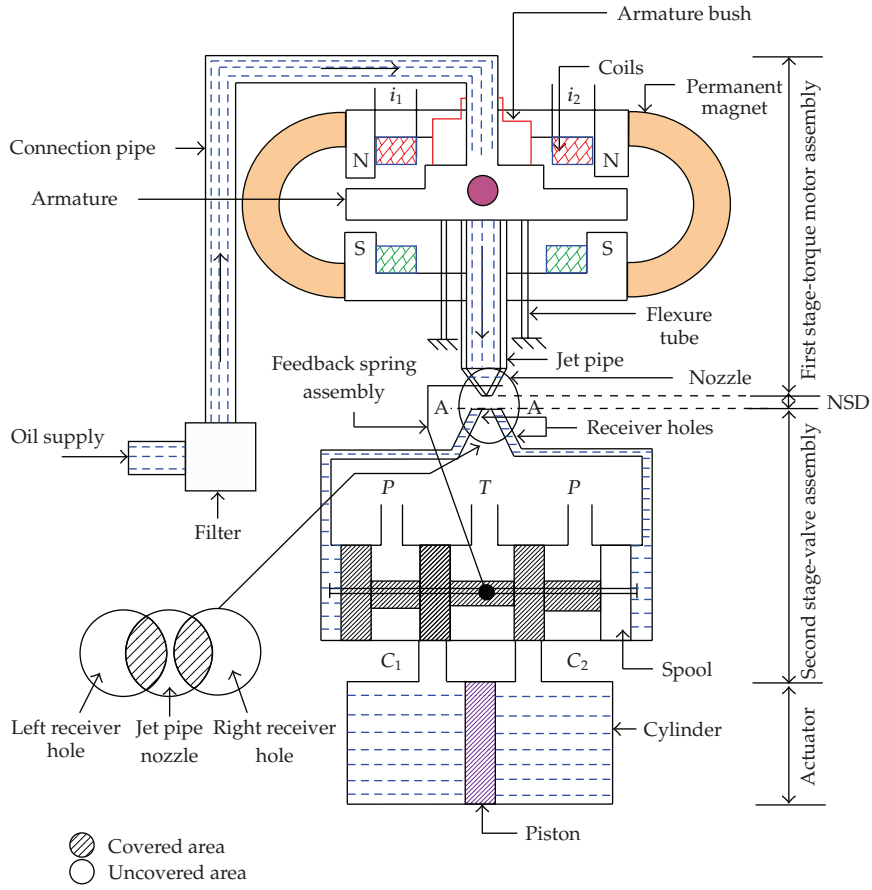

Figure 1: Schematic diagram of a jet pipe electrohydraulic servovalve.

EHSV because of large null flow, slower response, and rather unpredictable characteristics. Its main advantage lies in its insensitivity to dirty fluids.

1.1. Jet Pipe Electrohydraulic Servovalve

The schematic diagram of the analyzed jet pipe EHSV along with actuator is shown in Figure 1. It consists of two main assemblies-first-stage torque motor assembly and second-stage valve assembly. Between the first and the second stages, there is a mechanical feedback spring assembly to stabilize the valve operation. The analyzed jet pipe EHSV is of miniature type with the specifications shown in Table 1.

The jet pipe EHSV operation is as follows.

(i) At null position (no current input to the torque motor coils), the jet is directed exactly between the two receivers, making the pressures on both sides of the spool end equal. The force balance created by equal pressures in both end chambers holds the spool in a stationary position.

(ii) When a current passes through a torque motor coils, it generates an electromagnetic force (emf) on the armature ends and hence a torque on the armature and jet pipe.

Table 1: Specification of a jet pipe electrohydraulic.

No	Parameters	Value
1	System pressure	1.7 MPa
2.	Tank pressure	0.1 MPa
3.	Max. jet pipe deflection	0.2 mm
4.	Max. spool displacement	0.85 mm
5.	No load flow rate	17 L/min. for 1.7 MPa pressure drop
6	Spool diameter and length	11 mm and 40 mm
7.	Jet and receiver diameters	0.3 mm
8.	Piston diameter	54 mm
9.	Piston stroke length	100 mm
10.	Working fluid	Aviation kerosene

(iii) The torque rotates the jet pipe assembly around a pivot point and hence the fluid jet is directed to one of the two receiver holes in the receiver plate, creating a higher pressure in the spool end chamber connected to that receiver. The differential pressure pushes the spool in opposite direction to the jet pipe deflection.

(iv) As the spool starts moving, it pushes the feedback spring assembly, creating the restoring torque on the jet pipe to bring it back to the null position. When the restoring torque due to spool movement equals the applied torque on the armature, the spool stops at a particular position, until the value of the applied current is changed or the polarity of the applied current reversed. The resulting spool position opens a specified flow passage at the control ports of the second-stage to actuator.

The main investigations carried out on the jet pipe EHSV are no-load flow and load flow analysis. The obtained results are used in finite element analysis.

2. Theoretical Flow Modeling

The main purpose of the servovalve is to regulate precisely the required amount of fluid flow to the actuator to control the load position. The actuator load positioning depends on how fast the servovalve responds to the input signal. Two important recommended tests to study the valve performance are no-load and load flow characteristics. Both these are obtained through static analysis.

2.1. No-Load Flow Analysis

The standard procedure to ascertain the no-load flow for the servovalve is to connect the control ports C_1 and C_2 shown in Figure 2. As the spool starts moving, the control ports are opened and fluid flows from the supply port (P) to tank port (T). The amount of fluid flow depends on the opened port area and the differential pressure across the ports. Assuming a symmetric valve configuration, the fluid flow to and from the ports is calculated using the orifice theory:

$$Q_{ac} = K_2\sqrt{\Delta P_{V1}} = K_2\sqrt{\Delta P_{V2}}, \tag{2.1}$$

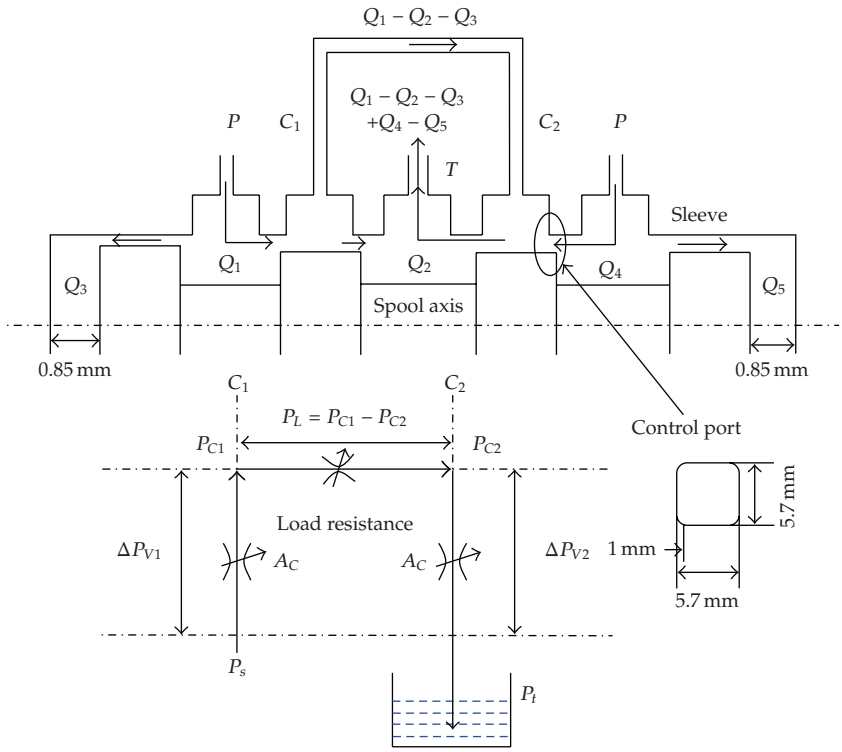

Figure 2: Port configuration for no-load flow analysis.

where $K_2 = C_d A_c \sqrt{2/\rho_o}$,

$$\begin{aligned} \Delta P_{V1} &= P_s - P_{C1}, \\ \Delta P_{V2} &= P_{C2} - P_t. \end{aligned} \tag{2.2}$$

Equating the above pressure drops for a symmetric valves,

$$P_s - P_t = P_{C1} - P_{C2}. \tag{2.3}$$

If a load resistance exists between C_1 and C_2, then the load pressure drop is given by

$$P_L = P_{C1} - P_{C2}. \tag{2.4}$$

By solving the (2.3) and (2.4), the control port pressures are given by

$$\begin{aligned} P_{C1} &= \frac{P_s + P_L + P_t}{2}, \\ P_{C2} &= \frac{P_s - P_L + P_t}{2}. \end{aligned} \tag{2.5}$$

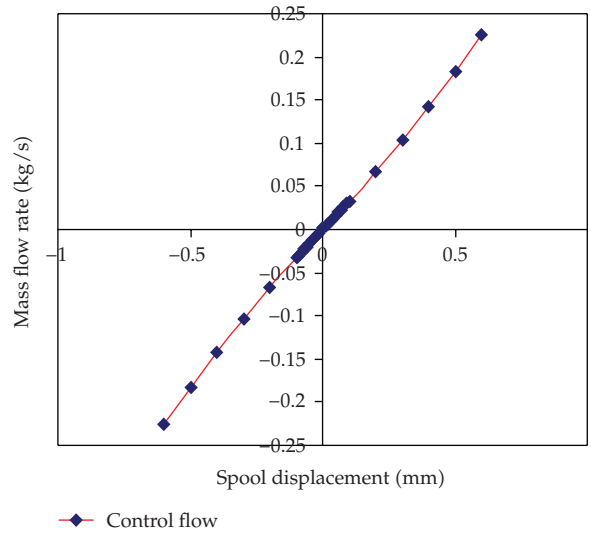

Figure 3: Mass flow rate in the no-load flow analysis.

Hence the valve pressure drops across the ports is given by

$$\Delta P_{V1} = \Delta P_{V2} = \frac{P_s - P_L - P_t}{2}. \tag{2.6}$$

The fluid flow to the actuator is given by

$$Q_{ac} = K_2 \sqrt{\frac{P_s - P_L - P_t}{2}}. \tag{2.7}$$

For the no-load flow analysis, the load pressure is $P_L = 0$, and so the control port pressures P_{C1} and P_{C2} are calculated from (2.5) and (7) as 0.9 MPa assuming the supply and tank pressures as 1.7 MPa and 0.1 MPa, respectively. The valve pressure drops, ΔP_{V1} and ΔP_{V2}, are obtained from (2.6) as 0.8 MPa. The flow through the control ports is calculated using (2.7). The variation of the control port area A_c with respect to the spool displacement is obtained from the solid model. Figure 3 shows the no-load mass flow rate variation with the spool displacement.

2.2. Load Flow Analysis

The flow analysis was carried out for different load conditions and flow is calculated using (2.7). The differential pressure across the valve is calculated using (2.6). Figure 4 shows the ideal normalized pressure-flow curves, of a jet pipe EHSV.

Corresponding to the input current to the torque motor there is a definite spool displacement. For the various spool displacements, there are different flow curves and they are all parabolas which pass through point 1 in either direction. To maximize the power

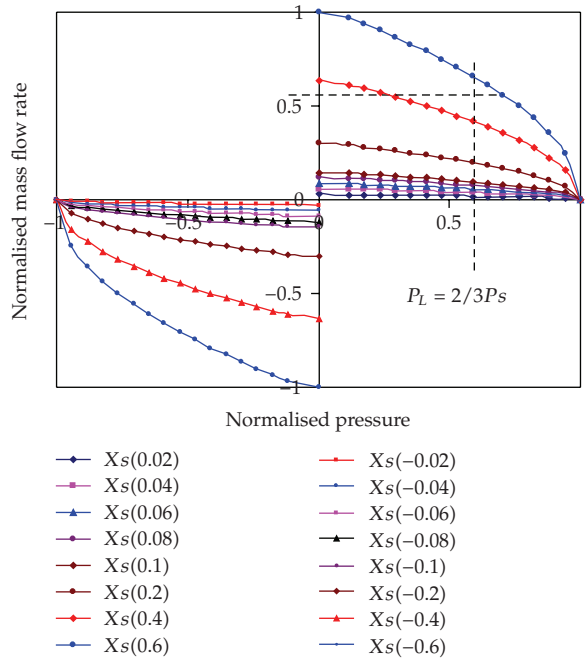

Figure 4: Mass flow rate in the load flow analysis.

output (H), the load pressure is 2/3rd of the supply pressure which provides sufficient flow to move the piston at the desired velocity [2].

3. Coupled Problems

Currently, solving coupled problems using FEM plays a major role in engineering field particularly in aerospace, mechanical and biomedical. In coupled problems, two or more physical systems interact with each other and independent solution of any one system being impossible without simultaneous solution of the others.

The coupled problems are classified as Class I and Class II depending on type of coupling that occur in the domains. In Class I type of problems, the coupling occurs in domain interfaces via the boundary conditions imposed at the interface, while in Class II problems domains overlap (totally or partially) and the coupling occurs through the governing differential equations [24].

The present paper aims to solve the Class I type problem that basically includes the Fluid-Structure-Interaction (FSI) where physically different domains (fluid and structure interaction or structure and structure interaction) interact with each other. The interfaces simply divide arbitrarily chosen regions in which different numerical discretization are used.

The examples of Class II problem are metal extrusion and soil dynamics. In the metal extrusion, the plastic flow is strongly coupled with the temperature field while at the same time the latter is influenced by the heat generated in the plastic flow. In earthquake response of a dam (Soil dynamics), the seepage flow and pressure interact with the dynamic behavior of the soil skeleton [24].

Modeling and analysis studies using numerical approach like FEM have not been carried out so far for the prediction of servovalve characteristics. The literature on applications of FEM to model the hydraulic components is limited. Some of the literature findings are as follows.

Tanaka and Sato [25] studied the affect of eddy current on the switching speed on/off and proportional solenoids by measuring the transient characteristics of the electric current and magnetic flux-flow, and next by calculating transient flux-flow on the process of permeating into the armature with the aid of newly programmed FEM.

Rosu and Vasiliu [26] applied the FE technique for the analysis of a swash plate axial piston pump components using the commercial FE code ANSYS. The analysis includes both static and dynamic study. The static analysis involved the study of static stresses and displacements of the yoke due to the hydrostatic pressure applied on the swash plate. The dynamic analysis includes the modal and transient analysis. The modal analysis revealed the natural frequencies and mode shapes of the components. The transient analysis revealed the response of the components under the action of a time-dependent pressure.

Meikandan et al. [27] and Sadashivappa [28] solved the 2D Reynold's equation, to determine the pressure distribution in the clearance between the piston and cylinder using the FEM. The film thickness equation for the clearance between the cylinder bore and the piston with form errors is introduced into the FEM formulation along with the operating parameters like piston velocity, supply pressure, viscosity of oil, and piston geometry. The program computes the pressure distribution around the circumference of the piston and the net centering force acting on the piston. Depending on the lateral load acting on the piston and the centering force developed, the eccentricity of piston inside the bore is determined. Here Galerkin's weighted residual method is used for obtaining the element equation.

4. Hydrostatic Fluid Model

In the present application of the actuator, it will be necessary to predict the mechanical response of a fluid-filled structure. The response of the structure depends not only on the external loads but also on the pressure exerted by the contained fluid. The major difficulty in these applications is the coupling between the structure and the fluid-filled cavity. In the present work, the mechanical structures are modeled with general purpose finite elements-beams, shells, and solids while the fluid cavities are modeled with special purpose hydrostatic fluid elements.

The general-purpose finite element formulation and their selection for different applications are widely elaborated by Cook [29]. The formulation of special-purpose hydrostatic fluid elements is detailed by Hibbitt et al. [30].

Hydrostatic fluid elements are surface elements that cover the boundary of the fluid cavity. Each cavity has a cavity reference node and has a single degree of freedom representing the pressure inside the fluid cavity. The cavity reference node is also used in calculating the cavity volume. The hydrostatic fluid elements appear as surface elements that cover the cavity boundary, but they are actually volume elements when the cavity reference node is accounted for. The fluid properties like bulk modulus, density, expansion coefficient, and so forth are defined properly for each cavity. The fluid inside the cavity can be compressible (pneumatic) or incompressible (hydraulic). The fluid volume of the cavity is a function of fluid pressure, fluid temperature, and fluid mass.

The volume $\overline{V}$ derived from the fluid pressure and temperature equals to the actual volume V of the cavity. In ABAQUS/Standard, this is achieved by augmenting the virtual work expression for the structure with constraint equation as

$$\overline{V} = f(p, \theta, m), \qquad V - \overline{V} = 0. \tag{4.1}$$

In addition, the virtual work contribution due to the cavity pressure is given by

$$\delta\Pi^* = \delta\Pi - p\delta V - \delta p\left(V - \overline{V}\right), \tag{4.2}$$

where $\delta\Pi^*$ is the augmented virtual work expression and $\delta\Pi$ is the virtual work expression for the structure without the fluid cavity. The negative signs imply that an increase in the cavity volume releases energy from the fluid. This represents a mixed formulation in which the structural displacements and fluid pressure are primary variables. The rate of the augmented virtual work expression is obtained as

$$\begin{aligned} d\delta\Pi^* &= d\delta\Pi - pd\delta V - dp\delta V - \left(dV - d\overline{V}\right)\delta p, \\ d\delta\Pi^* &= d\delta\Pi - pd\delta V - pd\delta V - dV\delta p + \frac{d\overline{V}}{dp}dp\delta p, \\ \delta\Pi^* &= \delta\Pi - p\sum_e \delta V^e - \delta p\left[\sum_e V^e - \sum_e \overline{V}^e\right], \end{aligned} \tag{4.3}$$

where $pd\delta V$ represents the pressure load stiffness, and $d\overline{V}/dp$ is the volume-pressure compliance of the fluid. Since the pressure is the same for all elements in the cavity, the augmented virtual work expression can be written as sum of the expressions for individual elements as

$$\delta\Pi^* = \sum_e \left[\delta\Pi^e - p\delta V^e - \delta p\left(V^e - \overline{V}^e\right)\right]. \tag{4.4}$$

Since the temperature is same for all elements in the cavity, the fluid volume can be calculated for each element individually as

$$\overline{V}^e = \overline{V}(p, \theta, m^e), \tag{4.5}$$

where m^e is the element mass. In the solution, the actual volume of the element may be different from the element volume as

$$V^e - \overline{V}^e \neq 0. \tag{4.6}$$

However, the total fluid volume will match the volume of the cavity. The fluid flow from one cavity to another cavity is modeled using two-node hydrostatic fluid link (FLINK), which is a function of the pressure difference, the average temperature, and the average pressure:

$$q = q\left(\Delta P, \overline{p}, \overline{\theta}\right). \tag{4.7}$$

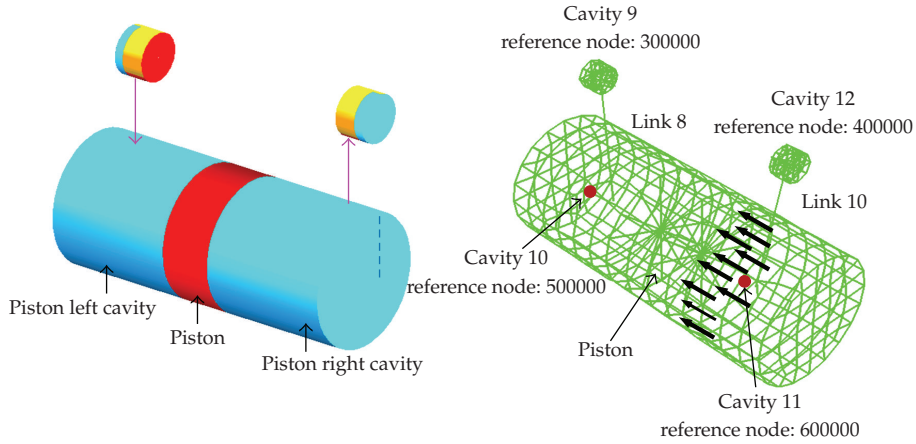

Figure 5: Solid and FE model of an actuator.

The flow rate needs to be integrated over a finite increment. The dependence on the average pressure is assumed to be weak. Hence, a semi-implicit method is used wherein Δp at the end of the increment and $\overline{p}^{o}$ at the start of the increment are used. For the temperature, $\overline{\theta}^{m}$ to be the average of $\overline{\theta}$ at the start and end of the increment is chosen, because this is likely to be the most accurate. Hence, the mass flow through the link is obtained as

$$\Delta m = q\left(\Delta P, \overline{p}^{o}, \overline{\theta}^{m}\right)\Delta t. \tag{4.8}$$

This mass change needs to be converted to a volume change in each cavity. It is assumed that the fluid in both cavities is the same, but the pressures (and possibly the temperatures) may be different. With the use of the pressure and the temperature-dependent density $\rho_i(p,\theta)$ for each cavity i, the relations become

$$\Delta\overline{V_1} = -\frac{\Delta m}{\rho_1}, \qquad \Delta\overline{V_2} = \frac{\Delta m}{\rho_2}. \tag{4.9}$$

5. Finite Element Modeling of Actuator

The finite element analysis carried out here to study the actuator under different external load conditions includes only the actuator and not the complete servovalve in order to study only the actuator dynamics. The fluid flow to the actuator for different load conditions is calculated and explained in Section 2. Figure 5 shows the solid and FE model of the actuator. Totally, there are four fluid cavities and two fluid links that are created. Cavity 9 and Cavity 12 correspond to the control port connections C_1 and C_2 which are in turn connected to either supply port or tank port depending on the servovalve spool displacement. Cavity 10 and Cavity 11 are piston end cavities. The piston is modeled with 3-dimensional 8-noded solid elements. A common boundary is created between the Cavity 10 and piston left face, similarly between Cavity 11 and piston right face. The FE model comprises of 402 elements, 582 nodes, and 3,356 variables.

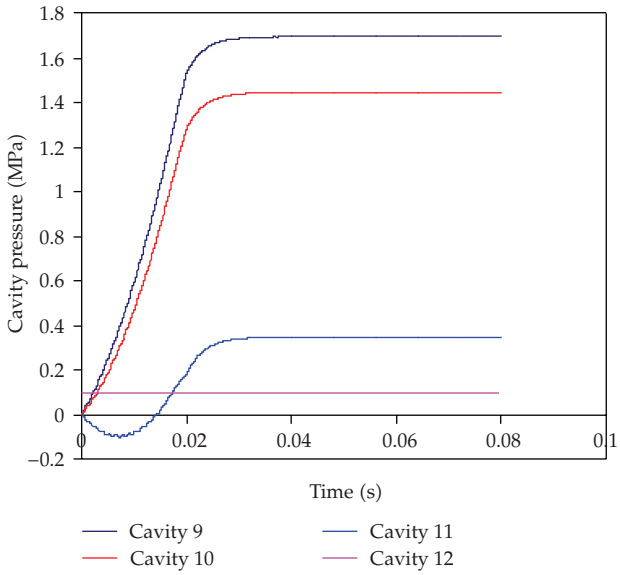

Figure 6: Variation of cavity pressures with time.

The FE analysis detailed here is for one load condition, which is selected as 2/3rd of the supply pressure of 1.7 MPa. Corresponding to this a distributed load (Dload) of 1.1 MPa is applied to the piston right face. In order to simulate the flow to the control ports C_1 or C_2, as the case may be, due to the displacement of the spool, a flux input (fluid) is added to the appropriate cavity. In the present case, the fluid flow responsible for the piston displacement is applied at Cavity 9 as a ramp input opposite to the applied Dload. The properties of the Links 8 and 10 are assumed to be same, about 0.2 MPa when full flow occurs through the link. As the flux is added to the Cavity 9, due to the fluid flow into the Cavity 10, the pressure in the Cavity 10 gradually increases. The variation of cavity pressures is shown in Figure 6.

Due to the application of the load on the right side face of the piston, initially the piston would have moved towards left, increasing the volume of Cavity 11 and at the same time reducing the volume of Cavity 10. Since no flow is present in any of the links, initially the pressure in the Cavity 11 shows a slight under pressure. As the flow into Cavity 10 starts, the pressure in this cavity starts increasing. At a value corresponding to the pressure required to overcome the load, the piston starts moving. From this point onwards, the pressure in the Cavity 11 also starts increasing due to a fluid flow through the Link 10 to the tank port (Cavity 12). The tank port (Cavity 12) pressure is maintained constant. When the steady state is reached, all the cavity pressures reach a constant value. The pressure difference between the pressures in the Cavity 9 and Cavity 10 as well as that between the Cavity 11 and Cavity 12 is equal and corresponds to the maximum pressure drop due to the flow input through Link 9 and that going out through Link 10. The two flows are same due to a symmetric actuator. The difference in pressure at the Cavities 10 and 11 corresponds to the load pressure drop.

The mass flow rate through the Links 8 and 10 is shown in Figure 7. As the fluid flows through the Link 8, it builds up pressure in the piston left side Cavity 10. After overcoming the applied load only, the piston starts displacing to right side and hence flows through Link 10 start after this delay.

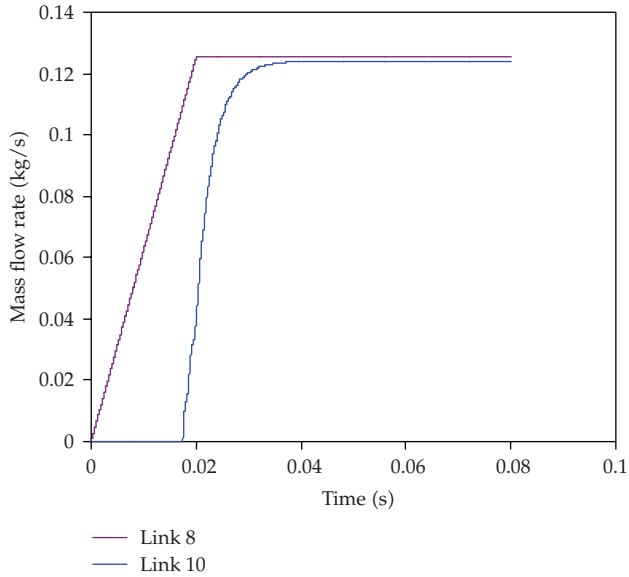

Figure 7: Variation of mass flow rate with time.

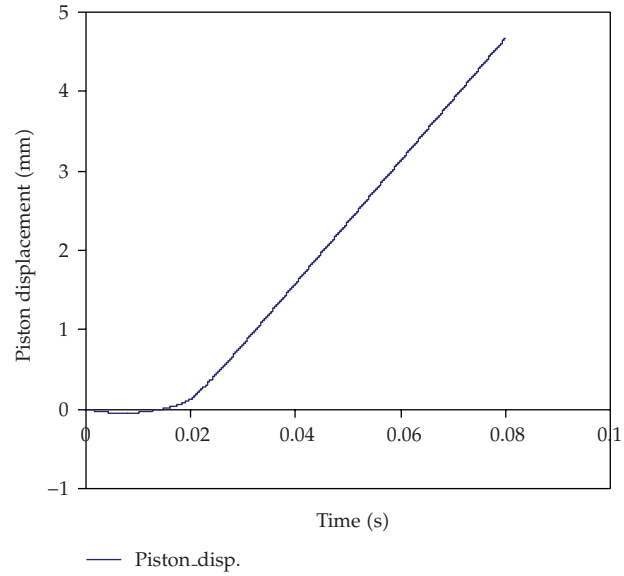

Figure 8: Variation of piston displacement with time.

Figure 8 shows the piston displacement and even here the above effect can be seen. The piston starts moving only when the pressure in the Cavity 10 overcomes the applied load. Due to the bulk modulus of the fluid, the piston is displaced slightly in the opposite direction and then it moves to the right side.

The piston velocity obtained from the FE simulation is compared with that obtained by dividing the flow rate by the area of cross section of the piston. This is shown in Figure 9.

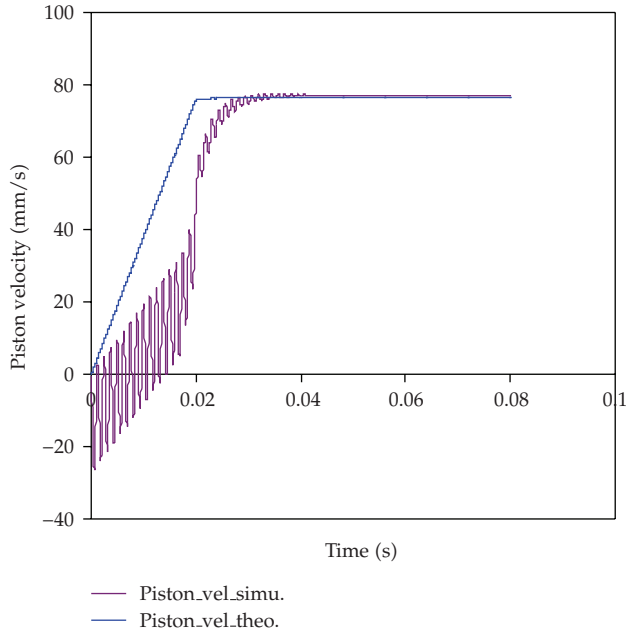

Figure 9: Comparison of piston velocity with time.

Even here, the piston velocity obtained through the FE simulation matches well with that calculated based on the fluid flow into the piston cavity and the piston area.

Figure 10 shows the piston end cavity volume variation. As stated earlier, as the piston starts moving, the cavity volume on the left side (Cavity 10) starts increasing and at the same time the cavity volume on the right side (Cavity 11) starts decreasing due to the piston displacement.

The bulk modulus of fluid affects the actuator dynamics. The variation in the bulk modulus is due to the air entrapment in the fluid flow. Hence, the analysis was extended to study the effect of change in the value of fluid bulk modulus.

Variation of piston displacement with time for different bulk modulus is shown in Figure 11. It is evident that as the bulk modulus reduces, the fluid compressibility increases and hence the delay in the start of the piston displacement increases.

6. Direct-Solution Steady-State Dynamics

Direct-solution steady-state dynamics is adopted to study the system's linearized response to harmonic excitation. The steady-state amplitude and phase of the system over the frequency range of excitation are obtained.

The main features of the direct-solution steady-state dynamic analysis [30] areas follows

(i) It is a linear perturbation procedure.

(ii) It calculates the response directly in terms of the physical degrees of freedom of the model.

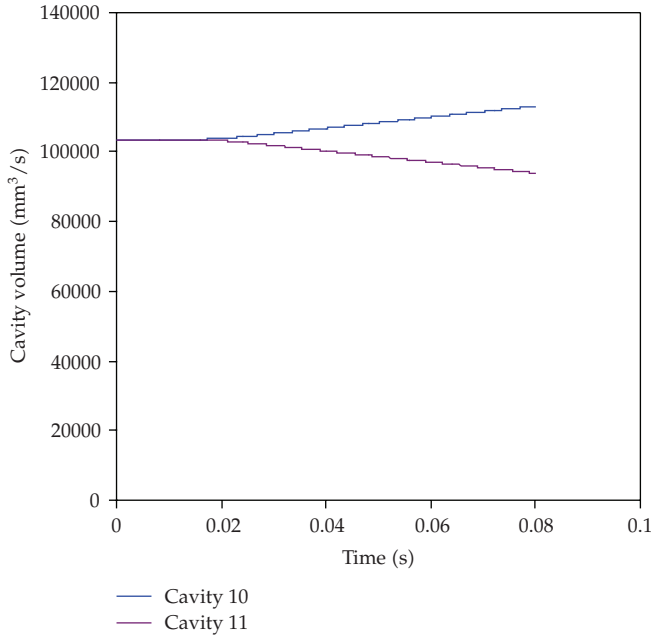

Figure 10: Variation of piston cavity volume with time.

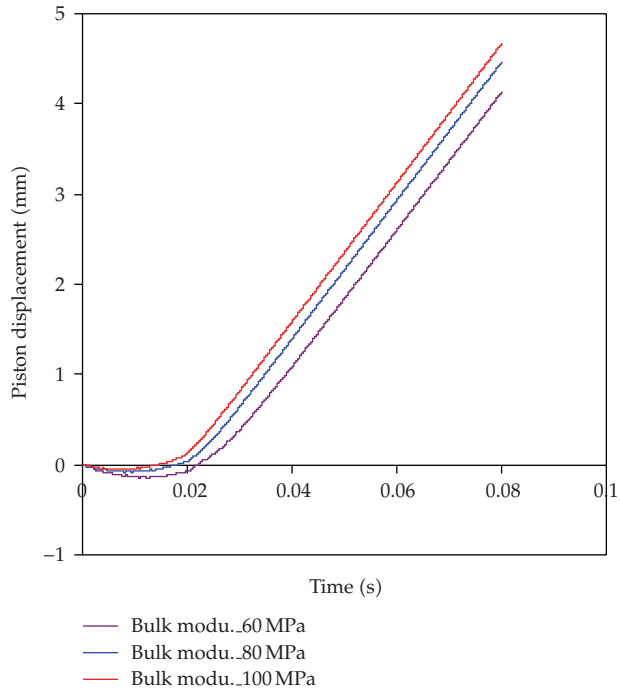

Figure 11: Variation of piston displacement for different bulk modulus with time.

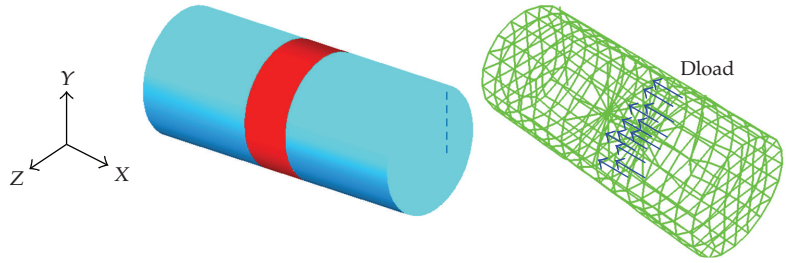

Figure 12: Solid and FE model of actuator.

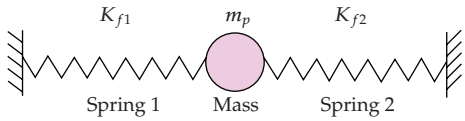

Figure 13: Simplified model of actuator: mass with two springs.

(iii) It is an alternative to mode-based steady-state dynamic analysis, in which the response of the system is calculated on the basis of the eigenmodes.

(iv) It is more expensive computationally than mode-based or subpace-based steady-state dynamics.

(v) It is more accurate than mode-based or subspace-based steady-state dynamics, in particular if significant frequency-dependent material damping or viscoelastic material behavior is present in the structure.

(vi) It is able to bias the excitation frequencies toward the approximate values that generate a response peak.

This procedure can be used in the following cases, for which the eigenvalues cannot be extracted using the mode-based analysis:

(i) for nonsymmetric stiffness

(ii) when any form of damping other than modal damping must be included,

(iii) when viscoelastic material properties must be taken into account.

7. Finite Element Modeling of an Actuator for Harmonic Excitation

Figure 12 shows the solid and FE model of the actuator. Figure 13 shows the simplified model of actuator. It consists of a mass with two springs. These two springs correspond to piston end fluid columns. The actuator considered here has an effective piston diameter of 51.84 mm, piston mass of 0.32 kg, and a stroke length of 50 mm on either side of the null position. The piston end cavities are modeled with 3-dimensional hydrostatic fluid elements and the piston with 3-dimensional 8-noded brick elements. The FSI is achieved using the common boundary between the piston end faces and fluid cavities. This is achieved while creating the fluid element by using the nodes of the piston end faces. The FE model comprises of 402 elements, 582 nodes, and 3356 variables.

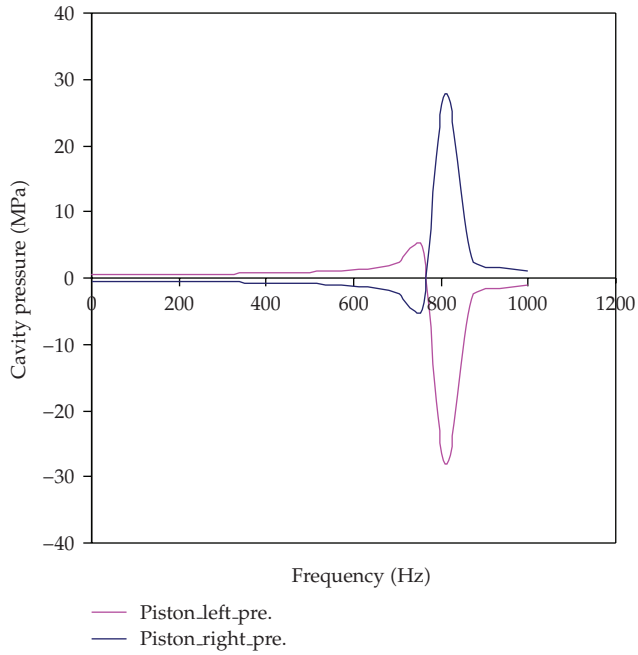

Figure 14: Variation of cavity pressure with frequency.

A distributed force of 1.1 MPa is applied on the right piston face. The frequency is swept from 1 to 1000 Hz. The variation of cavity volume and cavity pressure as well as the piston response is plotted. Figure 14 shows the variation of cavity pressure with frequency. The maximum pressure of 28 MPa in both cavities occurs at a frequency of 811 Hz. For particular combination of load on the piston and fluid bulk modulus, the appearance of the first peak is observed in Figure 14. This analysis is carried out for 100 MPa fluid bulk modulus. Figure 15 shows the variation of cavity pressure with frequency. This analysis is carried out for 80 MPa bulk modulus of fluid.

Figure 16 shows the variation of cavity volume on either side of the piston. It may be observed that maximum cavity volume of 29000 mm^3 occurs at a frequency of 811 Hz.

Figure 17 shows the piston response and the peak amplitude of 14 mm occurs at the same frequency of 811 Hz as before. It is an established fact that the natural frequency of the actuator depends on the piston positions and bulk modulus of the fluid [6, 7]. This was simulated and compared with the theoretical results. The FE simulation has been carried out for different piston position and bulk modulus and the results are shown in Figure 18.

Theoretical equation for calculating the natural frequency of a hydraulic cylinder is given by

$$\overline{\omega}_n = \sqrt{\frac{\beta}{m_p}\left[\frac{A_{AL}^2}{V_{AL}} + \frac{A_{AR}^2}{V_{AR}}\right]}. \tag{7.1}$$

The natural frequency of the actuator changes as the piston moves since the left and right cavity volume of the piston changes. The natural frequency of the actuator is

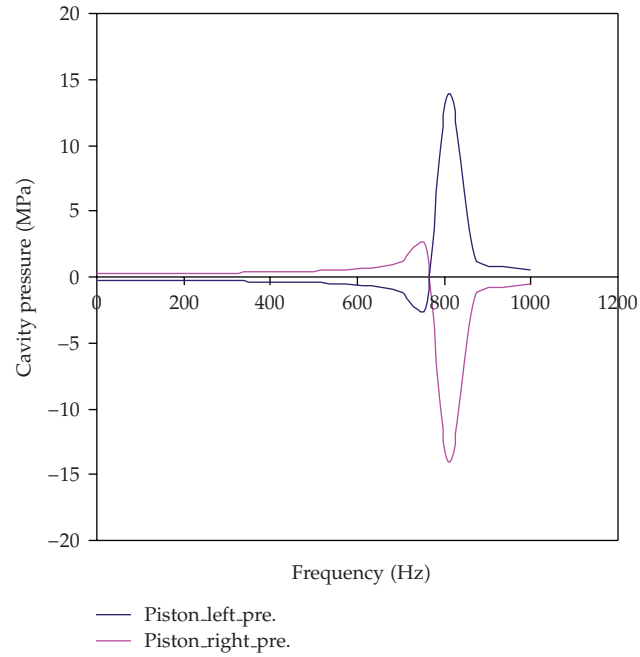

Figure 15: Variation of cavity pressure with frequency.

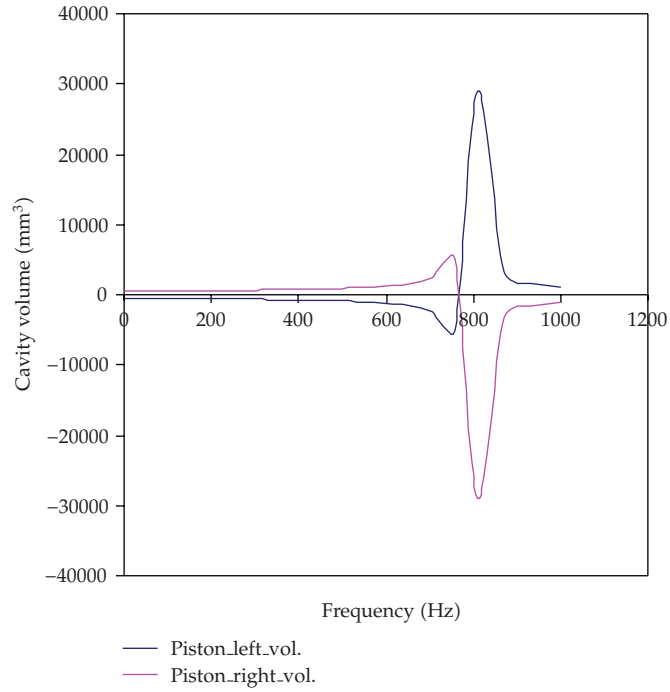

Figure 16: Variation of cavity volume with frequency.

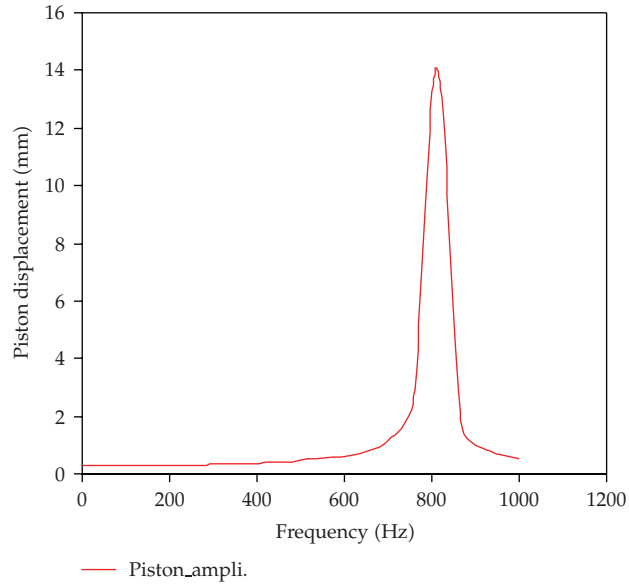

Figure 17: Frequency response of piston.

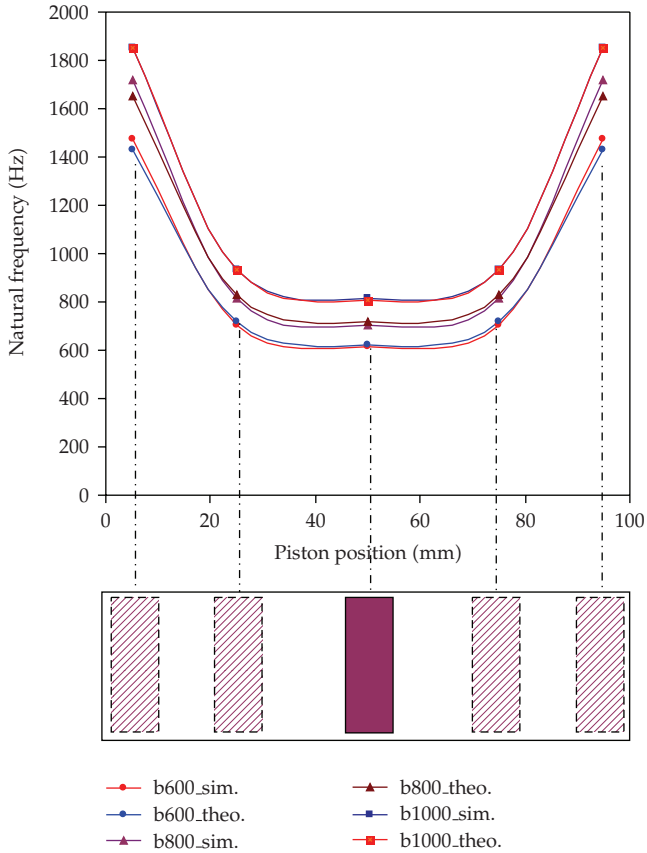

Figure 18: Variation of natural frequency of piston with piston position.

a maximum when the piston is fully retracted and decreases to a minimum at some point in the stroke and then increases to maximum as the piston approaches the end of the stroke. For a symmetric actuator the minimum natural frequency occurs when the piston is in mid position. The closeness of the theoretical and simulation results is observed (Figure 18).

8. Conclusions

(i) Finite element approach was adopted to model the fluid-structure interaction of servovalve component-actuator.

(ii) The dynamics of the jet pipe servovalve actuator was presented as the variation of cavity pressure, cavity volume, mass flow rates, and the actuator velocity with time.

(iii) The effect of bulk modulus was observed—as bulk modulus reduces, the fluid compressibility increases and hence the delay in the start of the piston displacement increases.

(iv) It was observed that the natural frequency of the actuator changes as the piston moves since the left and right cavity volume of the piston changes.

(v) The natural frequency of the actuator is a maximum when the piston is fully retracted and decreases to a minimum at some point in the stroke and then increases to maximum as the piston approaches the end of the stroke.

(vi) The natural frequency as obtained through FE modeling is well matched with theoretical modeling.

Notation

A_C: Control port area, mm^2
A_{AL}, A_{AR}: Actuator left side and right side cavity area, mm^2,
C_1, C_2: Control ports
Q_{ac}: Mass flow rate through the actuator, kg/s
Q_1 *to* Q_5: Fluid flow at the second-stage spool valve, l/min.
P: Pressure port
K_{f1}, K_{f2}: Fluid column spring stiffness, N/mm
m_a: Actuator mass, kg
m_p: Piston mass, kg
P_{C1}, P_{C2}: Control port pressure, MPa
P_L: Load pressure, MPa
P_s: Supply pressure, MPa
P_t: Tank pressure, MPa
T: Tank port
V_{AL}, V_{AR}: Actuator left side and right side cavity volume, mm^3
ΔP_{V1}: Valve pressure drop between the supply port and control port C_1, MPa
ΔP_{V2}: Valve pressure drop between the control port C_2 and tank port, MPa
ω_n: Natural frequency of an actuator, Hz
β: Bulk modulus of oil, MPa
ρ_o: Density of oil, kg/mm^3.

References

[1] C. M. Allen, *Electrohydraulic Servomechanisms*, McGraw-Hill, London, UK, 1963.

[2] H. E. Merrit, *Hydraulic Control Systems*, John Wiley & Sons, Chichester, UK, 1967.

[3] R. H. Maskrey and W. J. Thayer, "A brief history of electrohydraulic servomechanisms," *Journal of Dynamic Systems, Measurement and Control*, vol. 100, no. 2, pp. 110–116, 1978.

[4] D. C. Clark, *Selection and Performance Criteria for Electrohydraulic Servodrives*, Moog Technical Bulletin no. 122, Moog, East Aurora, NY, USA, 1969.

[5] T. P. Neal, *Performance Estimation for Electrohydraulic Control System*, Moog Technical Bulletin no. 126, Moog, East Aurora, NY, USA, 1974.

[6] F. D. Norvelle, *Electrohydraulic Control Systems*, Prentice-Hall, Upper Saddle River, NJ, USA, 2000.

[7] T. J. Viersma, *Analysis, Synthesis and Design of Hydraulic Servosystems and Pipelines*, Elsevier, Amsterdam, The Netherlands, 1980.

[8] J. Watton, *Fluid Power Systems: Modeling, Simulation, Analog and Microcomputer Control*, Prentice-Hall, London, UK, 1989.

[9] R. Walters, *Hydraulic and Electro-Hydraulic Servo Systems*, Iliffe Books, London, UK, 1967.

[10] S. Lee and J. F. Blackburn, "Contribution to hydraulic control-1. Steady-state axial forces on control-valve pistons," *Transactions of the ASME*, vol. 74, no. 6, pp. 1005–1011, 1952.

[11] C. K. Taft and J. P. Twill, "An analysis of the three-way underlapped hydraulic spool servovalve," *Journal of Dynamic Systems, Measurement, and Control*, vol. 100, pp. 117–123, 1978.

[12] I. Lee, T. Kim, and A. Kitagawa, "A new linearized equation for modelling a servovalve in hydraulic control systems," in *Proceedings of the JFPS International Symposium on Fluid Power*, vol. 3, pp. 899–904, Nara, Japan, 2002.

[13] P. N. Nikiforuk, P. R. Ukrainetz, and S. C. Tsai, "Detailed analysis of a two-stage four-way electrohydraulic flow-control valve," *Journal of Mechanical Engineering Science*, vol. 11, pp. 168–174, 1969.

[14] S. LeQuoc, R. M. H. Cheng, and A. Limaye, "Investigation of an electrogydraulic servovalve with tuneable return pressure and drain orifice," *Transactions of the ASME*, vol. 276, no. 109, pp. 276–285, 1987.

[15] B. B. Das, S. K. Zachariah, and B. Sebastian, "Nonlinear modeling for launch vehicle electrohydraulic servo actuation system," in *Proceedings of the National Conference on Emerging Challenges in Fluid Power Technology*, pp. 1–9, 2003.

[16] J. J. Fredlake and M. R. Adams, "Electronic fuel controls for executive jet aircraft," Tech. Rep. 831478, SAE, 1983.

[17] S. L. Bruce, "Development of control surface actuation systems on various configurations of the F-16," Tech. Rep. 831483, SAE, 1983.

[18] H. E. Harschburger, "Development of redundant flight control actuation systems for the F/A-18 strike fighter," Tech. Rep. 831484, SAE, 1983.

[19] K. Ogata, *Modern Control Engineering*, Prentice-Hall, New Delhi, India, 4th edition, 2003.

[20] S. Z. Dushkes and S. L. Cahn, "Analysis of some hydraulic components used in regulators and servo mechanisms," *Transactions of the ASME*, pp. 595–601, 1952.

[21] J. U. Thoma, "Fluid mechanics, bond graphs and jet pipe servo valves," *Modeling and Simulation of Systems*, pp. 77–81, 1989.

[22] P. D. Henri, J. M. Hollerbach, and A. Nahvi, "An analytical and experimental investigation of a jet pipecontrolled electropneumatic actuator," *IEEE Transactions on Robotics and Automation*, vol. 14, no. 4, pp. 601–611, 1998.

[23] Moog Inc., *The Deflector Jet Servovalve*, Moog Technical Bulletin no. 121, Moog, East Aurora, NY, USA.

[24] O. C. Zienkiewicz and R. L. Taylor, *The Finite Element Method-I*, Butterworth–Heinemann, London, UK, 2000.

[25] H. Tanaka and Y. Sato, "FEM analysis and measurement on the eddy current in magnetic circuit of PWM on/off and proportional solenoid valves," in *Proceedings of the 3rd JHPS International Symposium*, pp. 385–390, 1996.

[26] C. Rosu and N. Vasiliu, "Researches on the main components of a positive displacement pump by FEM," in *Proceedings of the 2nd International FPNI—PhD Symposium*, pp. 1–6, Modena, Italy, July 2002.

[27] N. Meikandan, R. Raman, M. Singaperumal, and K. N. Seetharamu, "Theoretical analysis of tapered pistons in high speed hydraulic actuators," *Wear*, vol. 137, no. 2, pp. 299–321, 1990.

[28] K. Sadashivappa, *The effect of form errors on the performance of hydraulic actuators*, Ph.D. thesis, Indian Institute of Technology Madras, Chennai, India, 1996.

[29] R. D. Cook, *Concepts and Applications of Finite Element Analysis*, John Wiley & Sons, New York, NY, USA, 1974.

[30] *ABAQUS/Standard Finite Element Simulation Package (ver.6.4), Vols. I-III*, Hibbitt, Karlsson & Sorensen, Pawtucket, RI, USA, 2002.